ASCA and ROSAT observations of distant massive cooling flows

S.W. Allen[1], A.C. Fabian[1], A.C. Edge[1], M.W. Bautz[2], A. Furuzawa[3], Y. Tawara[3].

1. Institute of Astronomy, Madingley Road, Cambridge CB3 OHA
2. Center for Space Research, MIT, Cambridge MA, USA
3. Department of Astrophysics, Nagoya University, Chikusa-ku, Furo-cho, Nagoya 464, Japan

arXiv:astro-ph/9609201v1   30 Sep 1996

ABSTRACT

We present the results from a detailed ASCA/ROSAT X-ray study of three distant, massive cooling flows; Zwicky 3146 ($z = 0.291$), Abell 1835 ($z = 0.252$) and E1455+223 (Zwicky 7160; $z = 0.258$). Using multiphase models fitted to the ASCA spectra, we determine values for the temperature, metallicity, luminosity and cooling rates in the clusters. These results are combined with deprojection analyses of the ROSAT images to provide detailed constraints on the mass distributions in the systems, and on the properties of their cooling flows. The spectral and imaging data identify these clusters as the three most-massive cooling flows known, with mass deposition rates of $\sim 1400, 2300$, and 1500 $M_\odot \, yr^{-1}$ respectively. We highlight the need for multiphase models to consistently model the spectral and imaging X-ray data, and discuss the importance of using these models in X-ray determinations of the cluster masses. We also present results from an extensive optical study of the clusters and report the discovery of a gravitational arc in Abell 1835. The lensing data provide an independent constraint on the distribution of mass in the cluster, in good agreement with the results from the multiphase (although not single-phase) X-ray analysis. We present measurements of the galaxy distributions in Abell 1835 and E1455+223 and relate these to the distributions of the total mass. The ASCA spectra place firm constraints on the column density of intrinsic X-ray absorbing material in the clusters. Abell 1835 and E1455+223 exhibit large intrinsic column densities ($N_H \sim 3-4 \times 10^{21}$ atom cm^{-2}) associated with their cooling flows. These clusters also exhibit significant amounts of reddening in the optical spectra of their central galaxies. The data for Zwicky 3146 indicate lower lower levels of X-ray absorption and reddening. All three clusters exhibit excellent alignment between the position angles of their X-ray emission and the optical emission from their dominant cluster galaxies.

Key words: galaxies: clusters: general – cooling flows – intergalactic medium – dark matter – gravitational lensing – X-rays: galaxies

1 INTRODUCTION

X-ray observations of clusters of galaxies show that in the central regions of most clusters the cooling time of the IntraCluster Medium (ICM) is significantly less than the Hubble time (*e.g.* Edge, Stewart & Fabian 1992). The observed cooling, which takes place primarily through the emission of X-rays, leads to a slow net inflow of material towards the cluster centre; a process known as a *cooling flow* (Fabian 1994).

Within the idealized model of an *homogeneous* cooling flow, all of the cooling gas flows to the centre of the cluster where it is deposited, having radiated away its thermal en-

ergy. However, observations of cooling flows show that the simple homogeneous model is not correct. Although the X-ray surface brightness profiles of clusters with cooling flows are substantially more sharply-peaked than those of non cooling-flow systems, the emission is not as sharply-peaked as it would be in the case of homogeneous flows. Rather than all of the cooling gas flowing to the very centres of the clusters, the X-ray data show that gas is 'cooling out' throughout the central few tens to hundreds of kpc. Typically the cooled material is deposited with $\dot{M}(r) \propto r$, where $\dot{M}(r)$ is the integrated mass deposition rate within radius r. The X-ray data firmly require that cooling flows are *inho-*

mogeneous with a range of density and temperature phases at all radii.

Spatially resolved X-ray spectroscopy of clusters also confirms the the presence of distributed cool (and rapidly cooling) gas in cooling flows. The spatial distribution and luminosity of the cool components determined from the spectral data are well-matched to values inferred from the X-ray images (*e.g.* Allen *et al.* 1993, Allen, Fabian & Kneib 1996; Fabian *et al.* 1996; Allen & Fabian 1996). For a detailed review of the theory and observations of cooling flows see Fabian (1994).

In this paper we present observations, made with the ASCA and ROSAT X-ray astronomy satellites, of three exceptionally luminous cluster cooling flows. Two of the systems, Zwicky 3146 ($z = 0.291$) and Abell 1835 ($z = 0.252$) were identified as X-ray luminous clusters during optical-follow up studies to the ROSAT All-Sky Survey (Allen *et al.* 1992a). The third system, E1455+223 (or Zwicky 7160; $z = 0.258$) was identified by Mason *et al.* (1981) in a follow-up to X-ray observations made with Einstein Observatory. All three clusters are included in the ROSAT Brightest Cluster Sample (Ebeling *et al.* 1996a).

Combining the high spectral resolution ASCA data with ROSAT images we present consistent determinations of the temperatures, metallicities, luminosities and cooling rates in the clusters. The data for Zwicky 3146, Abell 1835 and E1455+223 identify them as the three largest cluster cooling flows known to date. We constrain the level of intrinsic X-ray absorption in the cooling flows and relate the results to measurements of intrinsic reddening in the Central Cluster Galaxies (CCGs) of the systems. Results on the distributions of X-ray gas, galaxies, and the total gravitating matter in the clusters are reported.

The structure of this paper is as follows. In Section 2 we summarize the observations. In Section 3 we present the X-ray and optical imaging data and discuss the morphological relationships between the clusters and their CCGs. In Section 4 we discuss the spectral analysis of the X-ray data. In Section 5 present the results from the deprojection analyses of the ROSAT images. Section 6 discusses the optical properties of the clusters. In Section 7 we discuss some of the more important results in detail, and in Section 8 summarize our conclusions. Throughout this paper, we assume H_0=50 km s^{-1} Mpc^{-1}, $\Omega = 1$ and $\Lambda = 0$.

2   OBSERVATIONS

The details of the observations are summarised in Table 1. Exposure times for the ASCA data sets are effective exposures after standard data screening and cleaning procedures have been applied (Day *et al.* 1995). Hashed numbers following an instrument name indicate that those observations were carried out on more than one date. The ASCA observations of Abell 1835 were made in two parts, on consecutive days in 1994 July. The ROSAT HRI observations of Zwicky 3146 were carried out on 2 dates, in 1992 November and 1993 May, giving a total exposure of 26.0 ks. The HRI observations of E1455+223 were carried out in 3 parts, in 1992 January – 1994 July, with a total exposure time of 14.9 ks.

The ASCA observation of Zwicky 3146 was carried out in 1993 May during the PV stage of the mission. The SIS

detectors were used in 2-CCD mode with the target positioned approximately at the boundary between chips 1 and 2 in SIS0 (the nominal pointing position in 2-CCD mode during the PV phase). The observations of Abell 1835 and E1455+223 were carried out during the AO-1 stage of the ASCA program. These clusters were also observed in 2-CCD mode, but with the targets positioned more centrally in chip 1 of SIS0. For a detailed discussion of ASCA observing modes and instrument configurations see Day *et al.* (1995). Reduction of the ASCA data was carried out using the FTOOLS package. Standard selection and screening criteria were applied (Day *et al.* 1995). The ROSAT data were analysed using the STARLINK ASTERIX package.

The optical observations of Zwicky 3146 was carried out with the 3.6m telescope at the European Southern Observatory (ESO), La Silla, Chile. The ESO Faint Object Spectrograph Camera was used with the TEK 512×512 CCD (pixel scale 0.61 arcsec). An exposure of 120 sec in the R band was made in seeing of ~ 1.5 arcsec. The optical observations of Abell 1835 and E1455+223 were carried out with the 5m Hale Telescope, Palomar, as part of a follow up study (Edge *et al.* 1996) of the most X-ray luminous clusters in the ROSAT Brightest Cluster Sample. The COSMIC instrument and TEK 2048×2048 chip (pixel scale 0.28 arcsec) were used. Exposures of 1000 and 500 s were made in Gunn i, 500s and 600s in KC B, and 3000s in KC U, for Abell 1835 and E1455+223 respectively. The seeing was ~ 1.1 arcsec. The optical data were reduced and analysed in IRAF.

Figs. 1-3 show the optical images of the clusters, with the ROSAT HRI X-ray contours overlaid. (Details of the smoothing algorithms are given in the figure captions.)

3   MORPHOLOGY ANALYSIS

The images presented in Figs. 1-3, and the optical and X-ray co-ordinates listed in Table 2, demonstrate excellent agreement between the positions of the CCGs and the positions of the peaks of the X-ray emission from the clusters. [Errors of $\lesssim 5$ arcsec may be associated with the aspect solutions of the HRI data. The astrometry of the optical data is accurate to within 1 arcsec.]

The ellipticities and position angles of the X-ray emission from the clusters and the optical emission from the CCGs have been examined using the ELLIPSE isophote-analysis routines in IRAF. The images were re-binned to a suitable pixel size (8×8 arcsec^2 for the X-ray data and 0.57×0.57 arcsec^2 for the optical images) and were modelled with elliptical isophotes (Jedrzejewski 1987). The ellipticities, position angles and centroids of the isophotes were free parameters in the fits. The results are summarized in Table 3 where we list the mean ellipticities and position angles over the range of semi-major axes studied. We find excellent agreement between the position angles of the optical (CCG) and X-ray (cluster) isophotes.

The agreement between the position angles of the CCG and cluster isophotes, and the coincidence of the CCG co-ordinates and the peaks of the cluster X-ray emission, are similar to the results from studies of other large cooling-flow clusters at lower redshifts (White *et al.* 1994; Allen *et al.* 1995; Allen *et al.* 1996).

Table 1. Observation summary

Cluster	Instrument	Observation Date	Exposure (ks)
Zwicky 3146	ASCA SIS0	1993 May 18	26.3
	ASCA SIS1	” ”	31.6
	ASCA GIS2	” ”	30.2
	ASCA GIS3	” ”	30.2
	ROSAT HRI #1	1992 Nov 27	15.2
	ROSAT HRI #2	1993 May 17	10.8
	ROSAT PSPC	1993 Nov 13	8.62
	ESO 3.6m (R)	1992 Nov 11	0.12
Abell 1835	ASCA SIS0 #1	1994 Jul 20	18.2
	ASCA SIS1 #1	” ”	17.2
	ASCA GIS2 #1	” ”	13.0
	ASCA GIS3 #1	” ”	13.0
	ASCA SIS0 #2	1994 Jul 21	8.51
	ASCA SIS1 #2	” ”	8.22
	ASCA GIS2 #2	” ”	6.55
	ASCA GIS3 #2	” ”	6.56
	ROSAT HRI	1993 Jan 22	2.85
	ROSAT PSPC	1993 Jul 03	6.18
	Hale 5m (Gunn i)	1994 Jun 09	1.00
	Hale 5m (KC B)	1994 Jun 10	0.50
	Hale 5m (KC U)	1994 Jun 09	3.00
E1455+223	ASCA SIS0	1994 Jul 18	30.5
	ASCA SIS1	” ”	28.3
	ASCA GIS2	” ”	18.3
	ASCA GIS3	” ”	18.3
	ROSAT HRI #1	1992 Jan 11	4.09
	ROSAT HRI #2	1993 Jan 20	4.23
	ROSAT HRI #3	1994 Jul 07	6.57
	Hale 5m (Gunn i)	1994 Jun 10	0.50
	Hale 5m (KC B)	1994 Jun 10	0.60
	Hale 5m (KC U)	1994 Jun 10	3.00

Notes: Exposure times are effective exposures after all cleaning and correction procedures have been carried out. For Abell 1835 the ASCA observations were carried out in 2 parts, yielding total exposures of 26.7, 25.4, 19.6 and 19.6 ks for the S0, S1, G2 and G3 detectors, respectively. For Zwicky 3146, two separate ROSAT HRI observations were made, yielding a total exposure of 26.0 ks. For E1455+223 three HRI observations were carried out providing a total exposure of 14.9 ks.

Table 2. Target summary

Cluster	z	OPTICAL (J2000.)		X-RAY (J2000.)		F_X	L_X
		R.A.	Dec.	R.A.	Dec.		
Zwicky 3146	0.2906	$10^h23^m39.6^s$	$04°11'10''$	$10^h23^m39.8^s$	$04°11'11''$	6.6	2.8
Abell 1835	0.2523	$14^h01^m02.0^s$	$02°52'42''$	$14^h01^m01.9^s$	$02°52'43''$	12.3	3.8
E1455+223	0.2578	$14^h57^m15.1^s$	$22°20'31''$	$14^h57^m15.0^s$	$22°20'36''$	3.7	1.3

Notes: Redshifts and CCG coordinates (J2000) from Allen *et al.* (1992). X-ray coordinates denote the position of the X-ray peak determined from the HRI data. X-ray fluxes (F_X) in units of 10^{-12} erg cm^{-2} s^{-1} and luminosities (L_X) in 10^{45} erg s^{-1} are determined from the ASCA (S0) data. Fluxes are quoted in the 2-10 keV band of the observer. Luminosities are absorption-corrected and are quoted in the 2-10 keV rest-frame of the object.

Figure 1. The ESO 3.6m R band image of Zwicky 3146 with the ROSAT HRI X-ray contours overlaid. The optical data have a pixel scale of 0.61 arcsec and were taken in ~ 1.5 arcsec seeing. The X-ray image has a pixel size of 2×2 arcsec^2 and has been adaptively smoothed (Ebeling, White & Rangarajan 1996) to give ≥ 36 count smoothing element^{-1}. Contours are drawn at eight evenly-spaced logarithmic intervals between 0.89 and 22.38 ct pixel^{-1}.

Table 3. Isophote Analysis

Cluster	OPTICAL				X-RAY			
	pixel	range	ellipticity	P.A.	pixel	range	ellipticity	P.A.
Zwicky 3146	0.61×0.61	$1.2 - 3.7$	0.32 ± 0.01	125 ± 1	8.0×8.0	$16 - 24$	0.16 ± 0.04	127 ± 8
Abell 1835	0.57×0.57	$1.1 - 4.5$	0.21 ± 0.03	145 ± 4	8.0×8.0	$16 - 56$	0.20 ± 0.07	163 ± 16
E1455+223	0.57×0.57	$1.1 - 4.5$	0.16 ± 0.01	35 ± 2	8.0×8.0	$16 - 48$	0.20 ± 0.05	40 ± 7

Notes: A summary of the results from the isophote analysis of the optical (CCG) and X-ray (cluster) data. Columns (2) and (6) give the pixel sizes in arcsec of the re-binned optical and X-ray images used in the analyses. Columns (3) and (7) list the range (in arcsec) of semi-major axes analysed. Columns (4) and (8) give the mean ellipticities (defined as $1 - b/a$ where b and a are the semi-minor and semi-major axes respectively) of the optical and X-ray data in the regions analysed. Columns (5) and (9) list the mean position angles (PA) in degrees in these same regions.

4   SPECTRAL ANALYSIS OF THE ASCA DATA

4.1   Method of Analysis

SIS spectra were extracted from circular regions centred on the positions of the X-ray peaks. The radii of these regions were selected to minimize the number of chip boundaries crossed (and thereby minimize systematic uncertainties introduced into the data by such crossings) whilst covering as large a region of the clusters as possible. The compromise of these considerations lead to the choice of regions for spectral

Figure 2. The Hale 5m Gunn i image of Abell 1835 with the ROSAT HRI X-ray contours overlaid. The optical data have a pixel scale of 0.28 arcsec and were taken in $\sim$ 1.1 arcsec seeing. The X-ray image has a pixel size of 4×4 arcsec^2 and has been adaptively smoothed to give $\geq$ 16 count smoothing element^{-1}. Contours are drawn at six evenly-spaced logarithmic intervals between 0.79 and 7.94 ct pixel^{-1}.

Table 4. Regions included in the spectral analysis

Cluster	Detector	Radius (arcmin/kpc)
Zwicky 3146	SIS0	5.0/1620
	SIS1	4.0/1230
	SIS2	6.0/1940
	SIS3	6.0/1940
Abell 1835	SIS0	4.0/1190
	SIS1	3.0/890
	SIS2	6.0/1780
	SIS3	6.0/1780
E1455+223	SIS0	3.8/1140
	SIS1	2.8/840
	SIS2	6.0/1800
	SIS3	6.0/1800

analysis listed in Table 4. For Abell 1835 and E1455+223 the spectra were extracted from a single chip in each SIS (chip 1 in SIS0 and chip 3 in SIS1). For Zwicky 3146, which is centred on the boundary between chips 1 and 2 in SIS0 (chips 3 and 0 in SIS1), the data were extracted across the two chips in circular regions bounded by the outer chip edges. The GIS spectra used for the analysis of the cluster properties were extracted from circular regions of radius 6 arcmin (corresponding to $\sim$ 2 Mpc at the redshifts of the clusters) again centred on the peak of the X-ray emission from the clusters.

Background subtraction was carried out using the 'blank sky' observations compiled during the performance verification stage of the ASCA mission. (The blank sky observations are compiled from observations of high Galactic latitude fields free of bright X-ray sources). For X-ray sources lying in directions of relatively low Galactic column density, like the targets discussed in this paper, the blank sky observations provide a reasonable representation of the cosmic and instrumental backgrounds in the detectors over the energy ranges of interest.

The modelling of the X-ray spectra has been carried out using the XSPEC spectral fitting package (version 8.50; Shafer *et al.* 1991). For the SIS analysis, the 1994 Novem-

Figure 3. The Hale 5m Gunn i image of E1455+223 with the ROSAT HRI X-ray contours overlaid. The optical data have a pixel scale of 0.28 arcsec and were taken in ~ 1.1 arcsec seeing. The X-ray image has a pixel size of 2×2 arcsec^2 and has been adaptively smoothed to give ≥ 25 count smoothing element^{-1}. Contours are drawn at nine evenly-spaced logarithmic intervals between 0.21 and 8.32 ct pixel^{-1}.

ber 9 release of the response matrices from GSFC was used. Only those counts in pulse height analyser (PHA) channels corresponding to energies between 0.5 and 10 keV were included in the fits (the energies between which the calibration of the SIS is best-understood). For the GIS analysis, the 1995 March 6 release of the GSFC response matrices was used and only data in the energy range $1 - 10$ keV were included in the fits. All spectra were grouped before fitting to ensure a minimum of 20 counts per PHA channel, thereby allowing χ^2 statistics to be used.

The X-ray emission from the clusters has been modelled using the plasma codes of Raymond & Smith (1977; with updates incorporated into XSPEC version 8.50) and Kaastra & Mewe (1993). The results for the two plasma codes show good agreement. For clarity, only the results for the Raymond & Smith (hereafter RS) code will be presented in detail in this paper although the conclusions drawn may equally be applied to the analysis with the Kaastra & Mewe code.

We have modelled the ASCA spectra both by fitting the data from the individual detectors independently and by combining the data from all 4 detectors. The results from the fits to the individual detectors are summarised in Tables 5-7. When combining the data for the different detec-

tors the temperature, metallicity and column density values were linked together. However, the normalizations of both the ambient cluster emission and the cooling flow components were allowed to vary independently, due to the different source extraction areas used and residual uncertainties in the flux calibration of the instruments. The results from the fits to the combined data sets are summarized in Table 8.

4.2 The spectral models

The ASCA spectra were first examined with a simple single-phase model consisting of an RS component, to account for the X-ray emission from the cluster, and a photoelectric absorption component (Morrison & McCammon 1983) normalized to the equivalent Galactic hydrogen column density along the line-of-sight to the cluster. The free parameters in this model (hereafter Model A) were the temperature, metallicity and emission measure of the X-ray gas. The redshift of the X-ray emission from the cluster was fixed at the optically-determined values for the CCGs (Table 2).

We then examined a second model (Model B) in which the absorbing column density was also allowed to be a free

Table 5. Spectral Analysis of the ASCA data for Zwicky 3146

	Parameters	S0	S1	G2	G3
MODEL A	kT	$5.6^{+0.3}_{-0.3}$	$5.6^{+0.3}_{-0.4}$	$6.2^{+0.6}_{-0.6}$	$6.2^{+0.6}_{-0.6}$
	Z	$0.22^{+0.07}_{-0.06}$	$0.30^{+0.09}_{-0.08}$	$0.19^{+0.11}_{-0.11}$	$0.31^{+0.13}_{-0.11}$
	$N_{\rm H}$	0.34	0.34	0.34	0.34
	χ^2/DOF	243.7/235	256.1/207	182.3/209	173.9/214
MODEL B	kT	$5.9^{+0.7}_{-0.4}$	$5.6^{+0.6}_{-0.5}$	$6.5^{+0.6}_{-0.7}$	$6.3^{+0.8}_{-0.8}$
	Z	$0.22^{+0.07}_{-0.07}$	$0.30^{+0.10}_{-0.08}$	$0.19^{+0.11}_{-0.11}$	$0.32^{+0.12}_{-0.12}$
	$N_{\rm H}$	$0.16^{+0.15}_{-0.15}$	$0.34^{+0.18}_{-0.17}$	< 0.39	< 0.97
	χ^2/DOF	239.8/234	256.1/206	180.1/208	173.8/213
MODEL C	kT	$6.6^{+4.4}_{-1.0}$	$5.6^{+2.3}_{-0.5}$	$11.2^{+8.2}_{-5.0}$	$12.3^{+4.4}_{-5.8}$
	Z	$0.23^{+0.08}_{-0.07}$	$0.30^{+0.10}_{-0.09}$	$0.30^{+0.17}_{-0.19}$	$0.48^{+0.17}_{-0.19}$
	$N_{\rm H}$	$0.38^{+0.43}_{-0.30}$	$0.42^{+0.58}_{-0.24}$	< 1.29	$1.26^{+0.82}_{-0.96}$
	$\dot{M}$	< 2900	< 2800	< 2290	2240^{+260}_{-1760}
	χ^2/DOF	238.5/233	256.0/205	178.0/207	170.2/212
MODEL D	kT	$6.6^{+2.4}_{-0.9}$	$5.4^{+1.3}_{-0.5}$	$11.5^{+6.9}_{-5.1}$	$12.7^{+3.9}_{-6.1}$
	Z	$0.23^{+0.08}_{-0.08}$	$0.31^{+0.08}_{-0.09}$	$0.30^{+0.17}_{-0.17}$	$0.49^{+0.15}_{-0.20}$
	$N_{\rm H}$	0.34	0.34	0.34	0.34
	$\dot{M}$	1150^{+1400}_{-850}	< 1100	1740^{+570}_{-1340}	2240^{+250}_{-1740}
	$\Delta N_{\rm H}$	< 1.1	$U.C.$	< 2.44	< 5.43
	χ^2/DOF	238.6/233	255.5/205	177.9/207	170.2/212

Notes: The best-fit parameter values and 90 per cent ($\Delta\chi^2 = 2.71$) confidence limits from the spectral analysis of the ASCA data for Zwicky 3146. Temperatures (kT) are in keV and metallicities (Z) are quoted as a fraction of the Solar value (Anders & Grevesse 1989). Column densities ($N_{\rm H}$) are in units of 10^{21} atom cm^{-2} and mass deposition rates ($\dot{M}$) in $\rm M_\odot\,yr^{-1}$. χ^2 values and the number of degrees of freedom (DOF) in the fits are given for the four spectral models discussed in Section 4.2.

parameter in the fits. The fits to Abell 1835 and E1455+223 in particular showed highly significant improvements with the introduction of this single extra fit parameter. (Note that absorbing material was assumed to lie at zero redshift in this model). The best-fit parameter values and 90 per cent ($\Delta\chi^2 = 2.71$) confidence limits from the analyses with the single-phase models (A and B) are summarized in Tables 5–8.

Although the single-phase modelling can provide a useful parameterization of the properties of the cluster gas, the results obtained with such a model should be interpreted with caution. The deprojection analyses presented in Section 5 show that all three of the clusters discussed in this paper contain large cooling flows. The gas in the central regions of these clusters must therefore be highly multiphase *i.e.* contain a wide range of densities and temperatures at all radii.

We therefore next examined the data with more sophisticated spectral models in which the spectrum of the cooling flow was accounted for explicitly. The first of these models (Model C) consists of an RS component (to model the emission from the ambient ICM in the region of interest) and a cooling-flow component (following the models of Johnstone *et al.* 1992) modelling the X-ray spectrum of gas cooling from the ambient cluster temperature, to temperatures below the X-ray waveband, at constant pressure. Note that

Model C introduces only one extra free parameter into the fits relative to the single-phase Model B; the mass deposition rate of cooling gas. The upper temperature of the cooling gas, the metallicity, and the absorbing column density acting on the cooling flow were tied to those of the ambient cluster emission modelled by the RS component.

Fourthly, we examined a further cooling-flow model (D; which we expect to be the most physically-appropriate model) in which an intrinsic X-ray absorbing column density was associated with the cooling-flow. The excess absorption is modelled as a uniform absorbing screen in front of the cooling flow, at the redshift of the cluster, with the column density a free parameter in the fits. The column density acting on the ambient cluster emission was fixed at the Galactic value. The best-fit parameter values and confidence limits obtained with the multiphase, cooling-flow models (C,D) are also summarized in Tables 5–8.

Finally, a fifth model in which the X-ray emission from the cluster was parameterized by a combination of two RS components was studied. However, the statistical significance of including the second RS component in the fits (2 extra free parameters) is low and the results on the temperatures and emission measures of the two components, which are poorly constrained by the data, are not presented here.

Table 6. Spectral Analysis of the ASCA data for Abell 1835

	Parameters	S0	S1	G2	G3
MODEL A	kT	$9.4^{+0.7}_{-0.6}$	$9.4^{+1.1}_{-0.7}$	$6.5^{+0.7}_{-0.6}$	$6.8^{+0.6}_{-0.7}$
	Z	$0.24^{+0.10}_{-0.09}$	$0.26^{+0.12}_{-0.12}$	$0.26^{+0.13}_{-0.12}$	$0.23^{+0.12}_{-0.11}$
	$N_{\rm H}$	0.22	0.22	0.22	0.22
	χ^2/DOF	$416.7/369$	$363.5/298$	$200.0/216$	$199.5/261$
MODEL B	kT	$7.4^{+0.8}_{-0.6}$	$7.1^{+0.9}_{-0.7}$	$6.7^{+0.8}_{-1.0}$	$6.0^{+0.9}_{-0.7}$
	Z	$0.23^{+0.08}_{-0.07}$	$0.26^{+0.09}_{-0.09}$	$0.26^{+0.14}_{-0.12}$	$0.23^{+0.11}_{-0.10}$
	$N_{\rm H}$	$0.73^{+0.15}_{-0.14}$	$0.81^{+0.19}_{-0.19}$	< 0.82	$1.04^{+0.75}_{-0.69}$
	χ^2/DOF	$379.2/368$	$334.4/297$	$199.9/215$	$195.7/260$
MODEL C	kT	$8.8^{+6.6}_{-1.8}$	$7.2^{+5.0}_{-0.7}$	$12.1^{+3.3}_{-6.1}$	$6.0^{+6.1}_{-0.7}$
	Z	$0.26^{+0.09}_{-0.08}$	$0.26^{+0.08}_{-0.09}$	$0.34^{+0.17}_{-0.17}$	$0.23^{+0.13}_{-0.10}$
	$N_{\rm H}$	$1.04^{+0.32}_{-0.40}$	$0.81^{+0.33}_{-0.19}$	$1.03^{+0.83}_{-0.64}$	$1.05^{+1.07}_{-0.52}$
	$\dot{M}$	< 2600	< 2600	< 3500	< 4400
	χ^2/DOF	$377.4/367$	$334.4/296$	$198.3/214$	$195.7/259$
MODEL D	kT	$9.7^{+3.5}_{-1.2}$	$8.0^{+1.6}_{-1.2}$	$9.5^{+7.5}_{-3.6}$	$6.2^{+5.9}_{-0.9}$
	Z	$0.28^{+0.06}_{-0.08}$	$0.28^{+0.11}_{-0.10}$	$0.32^{+0.16}_{-0.16}$	$0.24^{+0.13}_{-0.11}$
	$N_{\rm H}$	0.22	0.22	0.22	0.22
	$\dot{M}$	2000^{+550}_{-450}	2000^{+1000}_{-600}	< 4300	< 4300
	$\Delta N_{\rm H}$	$3.25^{+2.25}_{-0.85}$	$6.68^{+5.50}_{-2.59}$	U.C.	U.C.
	χ^2/DOF	$372.9/367$	$327.2/296$	$198.9/214$	$195.5/259$

Notes: The best-fit parameter values and 90 per cent ($\Delta\chi^2 = 2.71$) confidence limits from the spectral analysis of the ASCA data for Abell 1835. Details as for Table 5.

4.3 Results from the spectral analysis

The results from the spectral analysis, presented in Tables 5–8, provide a consistent description of the X-ray properties of the clusters. We find good agreement in the results from the different detectors. Interestingly, in a reduced χ^2 sense, all four spectral models provide a statistically adequate description of the ASCA spectra. Even with the single-phase models, however, the statistical improvement obtained by allowing the X-ray absorption to fit freely (*i.e.* the improvement obtained with Model B over Model A) is very high – particularly for Abell 1835 and E1455+223 where a simple *F*-test (Bevington 1969) indicates the improvement to be significant at $>> 99.9$ per cent confidence. Model B indicates excess column densities (assumed to lie at zero red-shift) in Abell 1835 and E1455+223 of $5.0^{+1.1}_{-1.1} \times 10^{20}$ atom cm^{-2}and $5.9^{+1.7}_{-1.6} \times 10^{20}$ atom cm^{-2}, respectively. The data for Zwicky 3146 prefer a column density marginally less than the nominal Galactic value (Stark *et al.* 1992).

The introduction of the cooling flow component into the fits with Model C results in a further reduction in χ^2. However, the statistical significance of this improvement, relative to the model B results, is marginal, being required at > 95 per cent confidence only with the Abell 1835 data. (Note, however, that the improvement obtained with model C with respect to model A is very high.) In general, the lowest χ^2 values are obtained with Model D. However, it is difficult to interpret the improvement in χ^2 obtained with Model D with

respect to Models A–C in terms of a statistical significance since Model D includes fit parameters and constraints not present in the other models. Within the context of Model D the cooling flow component is required at high significance (Table 8). The data for Abell 1835 and E1455+223 also require significant amounts of intrinsic absorption associated with their cooling flows ($N_{\rm H} = 3.8^{+1.6}_{-0.4} \times 10^{21}$ atom cm^{-2}for Abell 1835 and $3.8^{+2.0}_{-0.8} \times 10^{21}$ atom cm^{-2}for E1455+223) whereas the data for Zwicky 3146 are consistent with Galactic absorption. Note that only the SIS data have the spectral resolution and sensitivity at lower energies ($E \lesssim 1$ keV) to detect the presence of cooling flows in the clusters. The GIS data do not provide firm constraints on the emission from cooling gas.

We conclude that the ASCA spectra alone are unable to discriminate at high significance between the multiphase cooling flow models (C, D) and the single-phase model (B) for the clusters. Although adopting Model D as intuitively the most reasonable description of the X-ray emission from the clusters leads to a strong spectral requirement for large cooling flows in all three systems, it is only through the combination of the spectral results with the results from the deprojection analyses discussed in Section 5, that the presence of massive cooling flows in these clusters is firmly established.

Finally in this Section, we note the possible effects of uncertainties in the low-energy calibration of the SIS data on our results. Our own analyses of ASCA observa-

Table 7. Spectral Analysis of the ASCA data for E1455+223

	Parameters	S0	S1	G2	G3
	kT	$5.0^{+0.4}_{-0.3}$	$5.4^{+0.5}_{-0.5}$	$4.5^{+0.8}_{-0.6}$	$4.5^{+0.6}_{-0.5}$
	Z	$0.29^{+0.10}_{-0.10}$	$0.14^{+0.11}_{-0.11}$	$0.20^{+0.23}_{-0.16}$	$0.39^{+0.24}_{-0.20}$
MODEL A	$N_{\rm H}$	0.31	0.31	0.31	0.31
	χ^2/DOF	$178.0/170$	$138.1/138$	$94.0/83$	$123.2/104$
	kT	$4.2^{+0.4}_{-0.3}$	$4.5^{+0.6}_{-0.5}$	$4.0^{+1.0}_{-0.8}$	$4.2^{+0.9}_{-0.7}$
	Z	$0.30^{+0.10}_{-0.09}$	$0.16^{+0.10}_{-0.10}$	$0.24^{+0.26}_{-0.21}$	$0.41^{+0.25}_{-0.20}$
MODEL B	$N_{\rm H}$	$0.89^{+0.23}_{-0.22}$	$0.89^{+0.29}_{-0.28}$	< 3.0	< 2.2
	χ^2/DOF	$157.7/169$	$125.1/137$	$92.5/82$	$122.4/103$
	kT	$5.3^{+2.3}_{-1.3}$	$5.5^{+4.1}_{-1.4}$	$7.1^{+3.1}_{-3.8}$	$4.6^{+5.5}_{-1.0}$
	Z	$0.32^{+0.10}_{-0.10}$	$0.16^{+0.11}_{-0.10}$	$0.34^{+0.25}_{-0.27}$	$0.43^{+0.35}_{-0.22}$
MODEL C	$N_{\rm H}$	$1.63^{+0.25}_{-0.25}$	$1.44^{+0.52}_{-0.75}$	$2.5^{+1.2}_{-2.2}$	< 3.3
	$\dot{M}$	< 3550	< 3500	< 2000	< 2390
	χ^2/DOF	$155.6/168$	$123.8/136$	$91.6/81$	$122.3/102$
	kT	$5.2^{+2.3}_{-0.8}$	$6.6^{+3.1}_{-1.9}$	$6.9^{+3.2}_{-3.7}$	$5.1^{+5.0}_{-1.6}$
	Z	$0.33^{+0.10}_{-0.10}$	$0.17^{+0.11}_{-0.11}$	$0.34^{+0.26}_{-0.26}$	$0.46^{+0.33}_{-0.24}$
MODEL D	$N_{\rm H}$	0.31	0.31	0.31	0.31
	$\dot{M}$	2290^{+1040}_{-960}	2500^{+750}_{-1100}	< 2320	< 2670
	$\Delta N_{\rm H}$	$3.8^{+4.2}_{-1.5}$	$2.6^{+4.0}_{-1.0}$	U.C.	U.C.
	χ^2/DOF	$154.1/168$	$124.0/136$	$91.4/81$	$122.3/102$

Notes: The best-fit parameter values and 90 per cent ($\Delta\chi^2 = 2.71$) confidence limits from the spectral analysis of the ASCA data for E1455+223. Details as for Table 5.

tions of bright, nearby X-ray sources indicate that the current GSFC response matrices (released 1994 November 9) may slightly overestimate the low-energy response of the SIS instruments. This systematic effect can lead to overestimates of Galactic column densities by $1 - 3 \times 10^{20}$ atom cm^{-2}(see also the discussion of calibration uncertainties associated with the ASCA instruments on the ASCA Guest Observer Facility World Wide Web pages at $http : //heasarc.gsfc.nasa.gov/docs/asca/cal\_probs.html$). Fixing the Galactic column densities in our analyses with spectral Model D at values 1.7×10^{20} atom cm^{-2}in excess of the nominal Galactic values for the clusters [1.7×10^{20} atom cm^{-2}being the best-fit systematic excess column density determined from our analysis of ASCA observations of the Coma cluster, which we expect to contain little or no intrinsic absorbing material (White *et al.* 1991, Allen & Fabian 1996), we determine best-fit intrinsic column densities for Zwicky 3146, Abell 1835 and E1455+223 of $N_{\rm H} < 0.6 \times 10^{21}$ atom cm^{-2}, $N_{\rm H} = 3.2^{+1.4}_{-0.6} \times 10^{21}$ atom cm^{-2}, and $N_{\rm H} = 3.1^{+1.9}_{-0.6} \times 10^{21}$ atom cm^{-2}, respectively. Hence, our conclusions on the presence of intrinsic absorbing material in these clusters are essentially unaffected by uncertainties in the calibration of the SIS instruments. Note that the temperature constraints are also little-affected by the calibration uncertainties, with the best-fit temperatures and 90 per cent confidence limits from the column density-adjusted fits being $kT = 6.9^{+1.2}_{-0.7}$, $9.1^{+2.1}_{-1.3}$ and $5.2^{+2.2}_{-0.7}$ keV, respectively.

4.4 Single-phase and Multiphase temperature results

The most notable differences between the results obtained with the single-phase (Model B) and multiphase (Models C,D) models are in the temperature determinations for the clusters. The cooling flow models imply significantly higher ambient cluster temperatures, and therefore larger integrated cluster masses.

The presence of a cooling flow will naturally lead to differences between the mean emission-weighted and mass-weighted temperatures for a cluster. The X-ray emissivity of the cooler, denser material in the cooling flow will be significantly higher than that of the surrounding hotter gas. The mean emission-weighted temperature will therefore be biased to temperatures below the mass-weighted value for the system. The effects of emission-weighting become particularly important for observations made with the comparatively low spectral resolution and limited ($0.1 - 2.4$ keV) bandpass of the ROSAT PSPC. In Table 9 we present the results from a spectral analysis of the PSPC data for the central 6 arcmin radius regions of Zwicky 3146 and Abell 1835. The single-phase models again provide a statistically adequate description of the spectra ($\chi^2_\nu \sim 1.0$) but the measured emission weighted temperatures are only $3.2^{+1.4}_{-0.7}$ keV and $3.8^{+1.6}_{-0.9}$ keV respectively, much less than $6.6^{+1.1}_{-0.7}$ keV and $9.5^{+1.3}_{-1.7}$ keV determined from the multiphase analysis of the ASCA spectra (Model D). The importance of distinguishing

Table 8. All instruments combined together

	Parameters	Model A	Model B	Model C	Model D
Zwicky 3146	kT	$5.74^{+0.19}_{-0.18}$	$6.07^{+0.33}_{-0.33}$	$6.9^{+2.7}_{-0.9}$	$6.6^{+1.1}_{-0.7}$
	Z	$0.26^{+0.05}_{-0.04}$	$0.26^{+0.04}_{-0.05}$	$0.27^{+.05}_{-0.05}$	$0.27^{+0.05}_{-0.05}$
	N_H	0.34	$0.17^{+0.12}_{-0.09}$	$0.54^{+0.34}_{-0.29}$	< 1.02
	$\dot{M}$	—	—	1870^{+1270}_{-1350}	1330^{+1220}_{-820}
	χ^2/DOF	$864.4/871$	$858.6/870$	$852.3/866$	$853.6/866$
Abell 1835	kT	$8.41^{+0.38}_{-0.39}$	$7.03^{+0.34}_{-0.33}$	$9.1^{+5.3}_{-1.6}$	$9.5^{+1.3}_{-1.7}$
	Z	$0.26^{+0.05}_{-0.05}$	$0.26^{+0.06}_{-0.05}$	$0.30^{+0.06}_{-0.06}$	$0.31^{+0.06}_{-0.05}$
	N_H	0.22	$0.72^{+0.11}_{-0.10}$	$1.12^{+0.24}_{-0.34}$	$3.8^{+1.6}_{-0.4}$
	$\dot{M}$	—	—	2050^{+1280}_{-1440}	2090^{+630}_{-700}
	χ^2/DOF	$976.4/958$	$909.2/957$	$898.7/953$	$891.8/953$
E1455+223	kT	$5.01^{+0.26}_{-0.26}$	$4.29^{+0.25}_{-0.24}$	$5.0^{+2.6}_{-0.7}$	$5.4^{+1.9}_{-0.7}$
	Z	$0.23^{+0.06}_{-0.07}$	$0.25^{+0.07}_{-0.06}$	$0.26^{+0.07}_{-0.06}$	$0.27^{+0.07}_{-0.07}$
	N_H	0.31	$0.90^{+0.17}_{-0.16}$	$1.48^{+0.45}_{-0.49}$	$3.8^{+2.0}_{-0.8}$
	$\dot{M}$	—	—	1890^{+1300}_{-1490}	2030^{+720}_{-880}
	χ^2/DOF	$541.8/501$	$503.5/500$	$498.8/496$	$498.2/496$

Notes: The best-fit parameter values and 90 per cent ($\Delta\chi^2 = 2.71$) confidence limits from the spectral analyses with data from all 4 detectors combined. Temperatures (kT) are in keV and metallicities (Z) are quoted as a fraction of the solar Value (Anders & Grevesse 1989). Column densities (N_H) are in units of 10^{21} atom cm^{-2}. kT, Z, and N_H are linked in the fits. However, the mass deposition rates for each detector ($\dot{M}$; quoted in $M_\odot$ yr^{-1}) are included as independent fit parameters, due to variations in source extraction area and uncertainties in the flux calibration of the instruments. The $\dot{M}$ value quoted for models C and D is for the S0 detector.

Table 9. PSPC spectra for Zwicky 3146 and Abell 1835

Parameter	Zwicky 3146	Abell 1835
kT	$3.2^{+1.4}_{-0.7}$	$3.8^{+1.6}_{-0.9}$
Z	$0.52^{+1.68}_{-0.48}$	$0.0^{+0.22}_{-0.0}$
N_H	$0.23^{+0.05}_{-0.06}$	$0.18^{+0.03}_{-0.02}$
χ^2/DOF	$26.3/22$	$17.0/20$

Notes: The best-fit parameter values and 90 per cent ($\Delta\chi^2 = 2.71$) confidence limits from the spectral analysis of the PSPC data.

between single-phase and multiphase models in the analysis of X-ray data for clusters is discussed in more detail in Section 7.1.
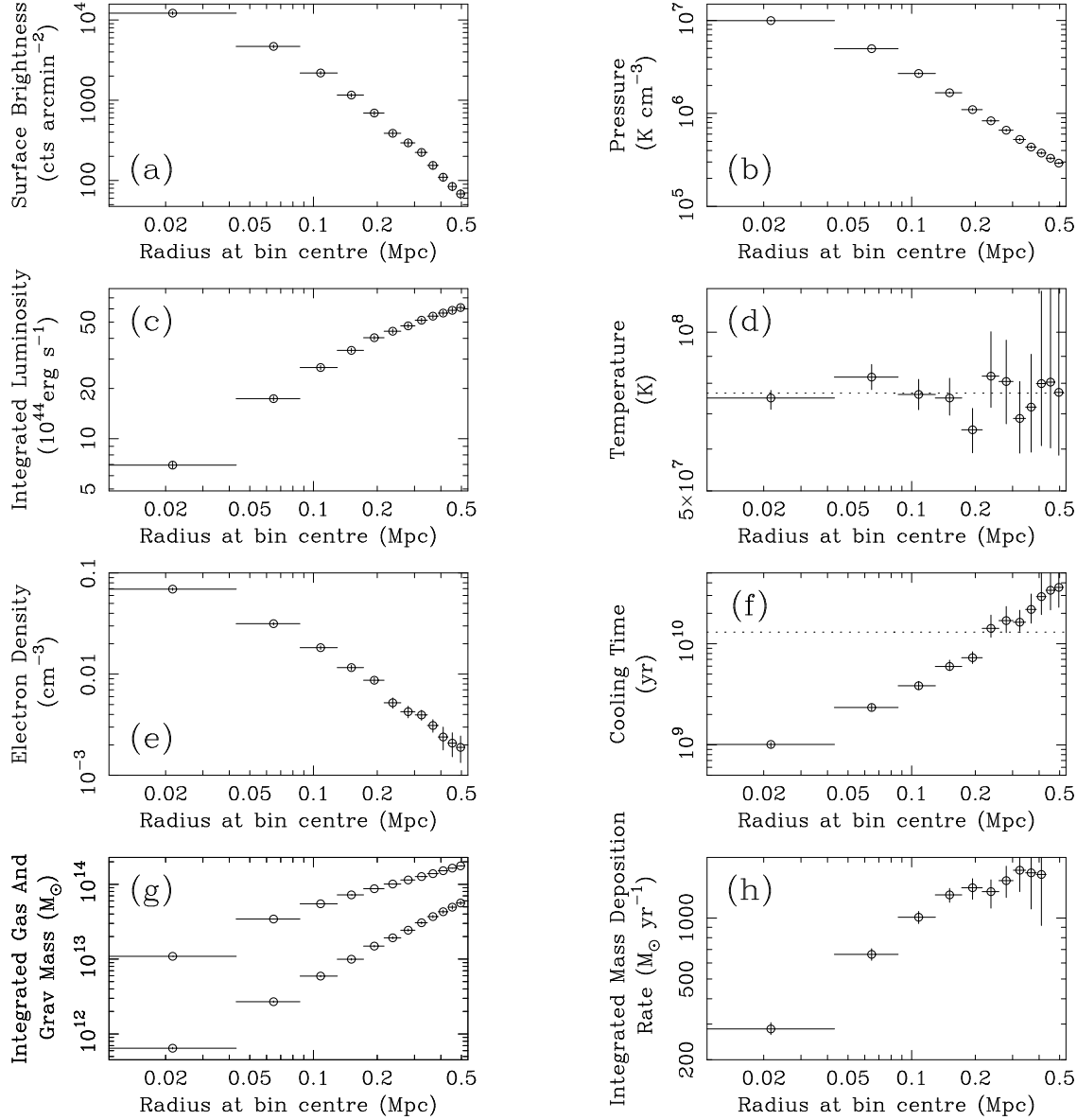
5   DEPROJECTION ANALYSIS

5.1   General results

We have carried out a deprojection analysis of the ROSAT images using an updated version of the code of Fabian *et al.* (1981). Using assumptions of spherical symmetry and hydrostatic equilibrium in the ICM, the deprojection technique

Table 10. Deprojection analyses of the clusters

	$t_{\rm cool}$	$r_{\rm cool}$	$\dot{M}$
Zwicky 3146	$1.01^{+0.06}_{-0.06}$	231^{+50}_{-37}	1355^{+408}_{-129}
Abell 1835	$1.36^{+0.31}_{-0.31}$	231^{+26}_{-13}	1106^{+455}_{-425}
E1455+223	$1.15^{+0.17}_{-0.15}$	213^{+47}_{-33}	732^{+162}_{-64}

Notes: A summary of the results from the deprojection analyses of the ROSAT HRI data. Cooling times ($t_{\rm cool}$) are mean values for the central (8 arcsec) bin and are in units of 10^9 yr. Cooling radii ($r_{\rm cool}$), the radii at which the cooling time exceeds the Hubble time (1.3×10^{10} yr), are in kpc. Integrated mass deposition rates within the cooling radii ($\dot{M}$) are in units of $M_\odot$ yr^{-1}. Errors on the cooling times are the 10 and 90 percentile values from 100 Monte Carlo simulations. The upper and lower confidence limits on the cooling radii are the points where the 10 and 90 percentiles exceed, and become less than, the Hubble time, respectively. Errors on the mass deposition rates are the 90 and 10 percentile values at the upper and lower limits for the cooling radius. Galactic column densities as listed in Table 1 are assumed.
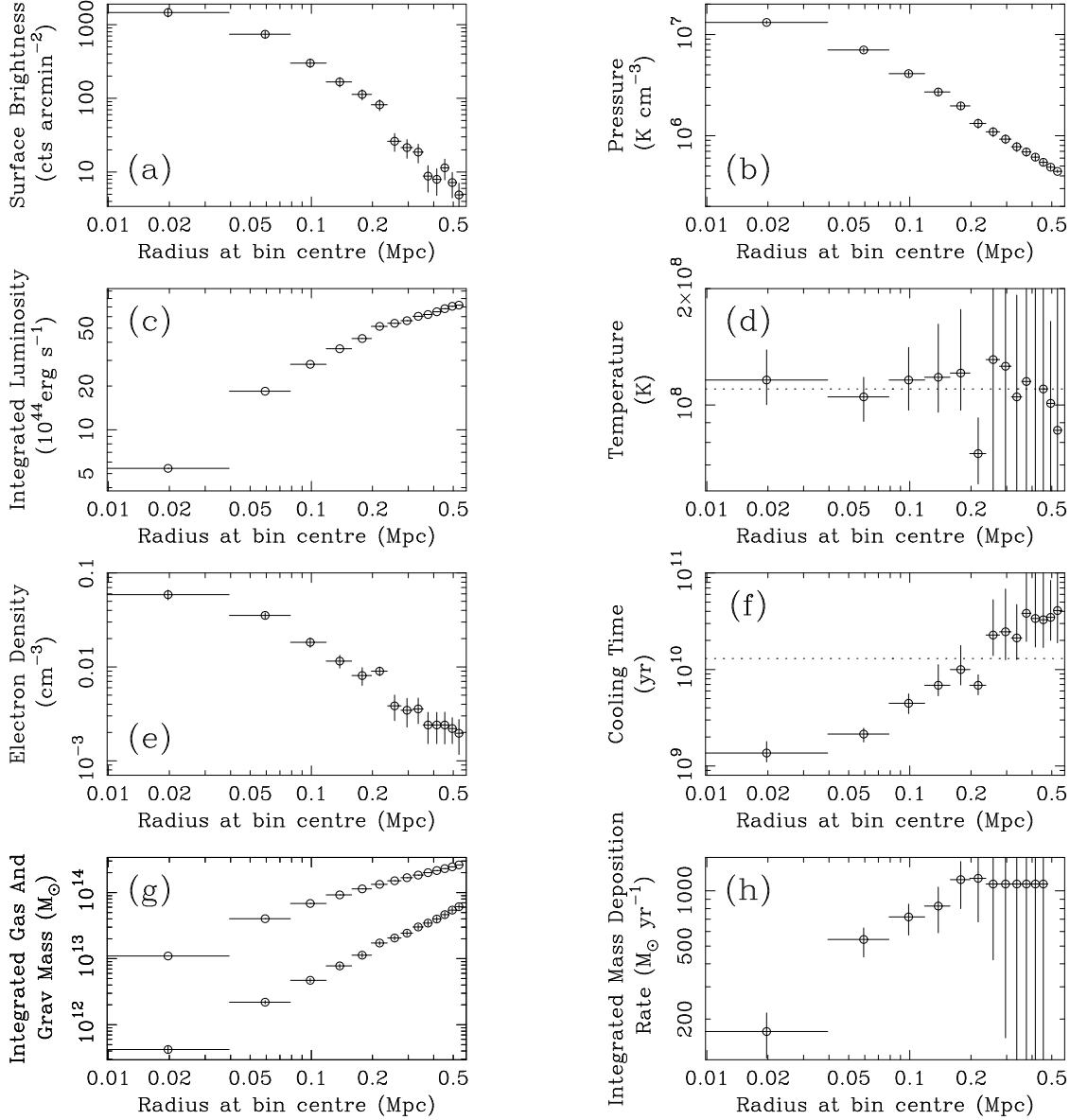
Figure 7. A summary of the results from the deprojection analysis of the HRI data for Zwicky 3146. From left to right, top to bottom, we plot; (a) surface brightness, (b) pressure, (c) integrated luminosity, (d) temperature, (e) electron density, (f) cooling time, (g) integrated gas and gravitational mass and (h) integrated mass deposition rate. Data points are mean values and 1σ errors (in each radial bin) from 100 Monte Carlo simulations, except for (d), (f) and (h) where the median and 10 and 90 percentile values have been plotted.

can be used to study the properties of the intracluster gas (*e.g.* density, pressure, temperature, cooling rate) as a function of radius. The deprojection method requires that either the total mass profile (which defines the pressure profile) or the gas temperature profile be specified. Following ASCA observations of nearby cooling flow clusters (Fabian *et al.* 1996), and the results from the combined X-ray and gravitational lensing study of the cooling-flow cluster PKS0745-191 (Allen *et al.* 1996), we assume that the mass-weighted temperature profiles in the clusters remain constant, at the

temperatures determined from the fits with the multiphase spectral models to the combined detector data sets (Table 8). Spectral model D is intuitively the preferred model, but using the full temperature range allowed by models C and D probably provides a more realistic estimate of the true uncertainty on the mass-weighted temperatures in the highly complex, multiphase environments of the cooling flows. Column densities were are fixed at the Galactic values from Stark *et al.* (1992), but see also Section 5.3.

The clusters discussed in this paper are remarkably

Figure 8. A summary of the results from the deprojection analysis of the HRI data for Abell 1835. Details as for Fig. 7

similar in their X-ray properties to PKS0745-191 and the analogy to that system is a reasonable one. It should be noted that although the deprojection method of Fabian *et al.* (1981) is essentially a single-phase technique, it produces results in good agreement with the more detailed multi-phase treatment of Thomas, Fabian & Nulsen (1987) and, due to its simple applicability at large radii, is better-suited to the present project.

The azimuthally averaged X-ray surface brightness profiles of the clusters determined from the HRI data (background-subtracted and corrected for telescope vignetting) and the results from the deprojection analyses are

summarized in Figs. 7−9. The primary results on the cooling flows in the clusters; the central cooling times, the cooling radii and the integrated mass deposition rates within the cooling radii are listed in Table 10. The results on the cooling flow in Zwicky 3146 are in good agreement with those reported by Edge *et al.* (1994) from an earlier analysis of the HRI data. The mass deposition from the cooling flows is distributed throughout the inner ~ 200 kpc of the clusters with $\dot{M} \propto r$. As noted in Section 1, such distributed mass deposition profiles requires that the central ICM is inhomogeneous (Nulsen 1986; Thomas, Fabian & Nulsen 1987; Fabian 1994). Note also that the mass deposition profiles
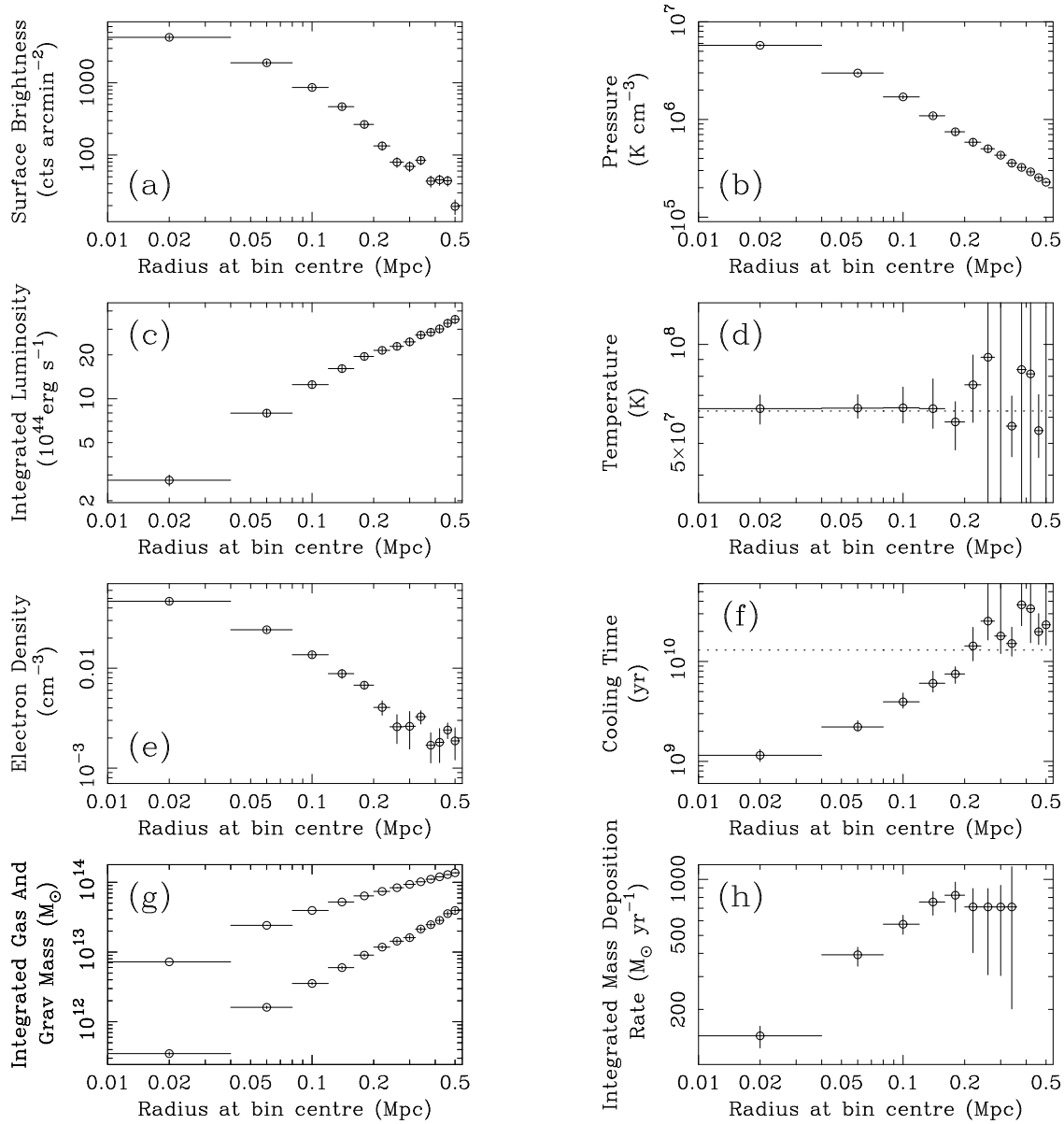
Figure 9. A summary of the results from the deprojection analysis of the HRI data for E1455+225. Details as for Fig. 7

shown in Figs. $7-9$(h) flatten at radii < 200 kpc, where the cooling time is $\lesssim 10^{10}$ yr. Thus accounting for the look-back time to the clusters ($\sim 4 \times 10^{9}$ yr) does not significantly alter the integrated mass deposition rates.

5.2 Parameterization of the cluster masses

In Table 11 we summarize the mass distributions required to produce the flat temperature profiles described in Section 5.1 We have parameterized the mass distributions as isothermal spheres (Equation 4-125 of Binney & Tremaine 1987) with core radii, r_c, and velocity dispersions, σ. In Fig. 11 we plot

the X-ray gas mass/total mass ratios for the central 500 kpc of the clusters (where the total mass is assumed to be described by the best-fit parameters listed in Table 11).

5.3 The correction for intrinsic absorption

As discussed in Section 5.1, for the purposes of deprojection we have assumed that the column densities to the clusters are given by the Galactic values of Stark *et al.* (1992). However, the spectral analysis of Section 4 clearly shows that both Abell 1835 and E1455+223 exhibit significant excess
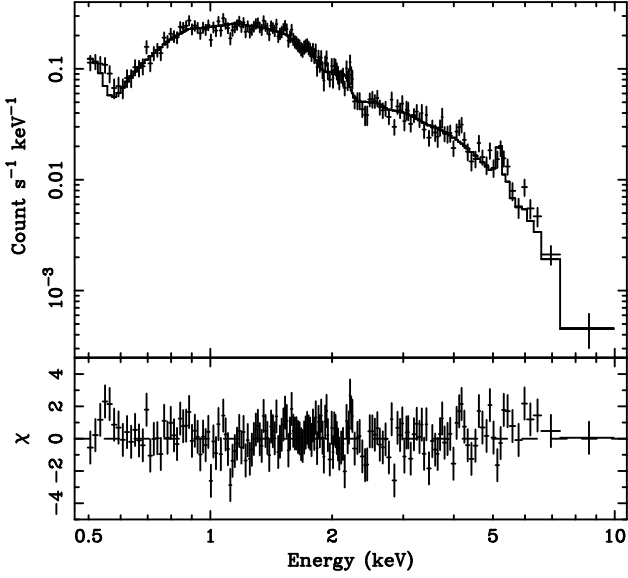
Figure 4. (Upper Panel) The S0 spectrum for Zwicky 3146 with the best-fit solution for Model B overlaid. The data have been binned-up by a factor 5 along the energy axis for display purposes. (Lower Panel) Residuals to the fit. The positive residuals at $E \sim 0.55$ keV are due to small systematic uncertainties in response matrix around the oxygen edge in the detector.
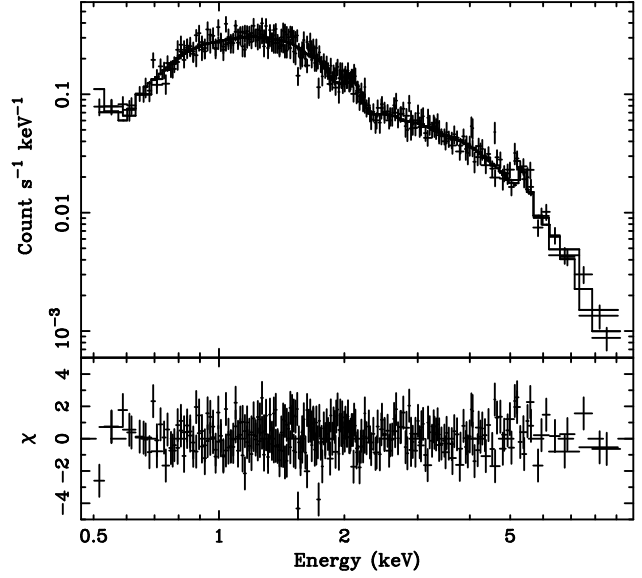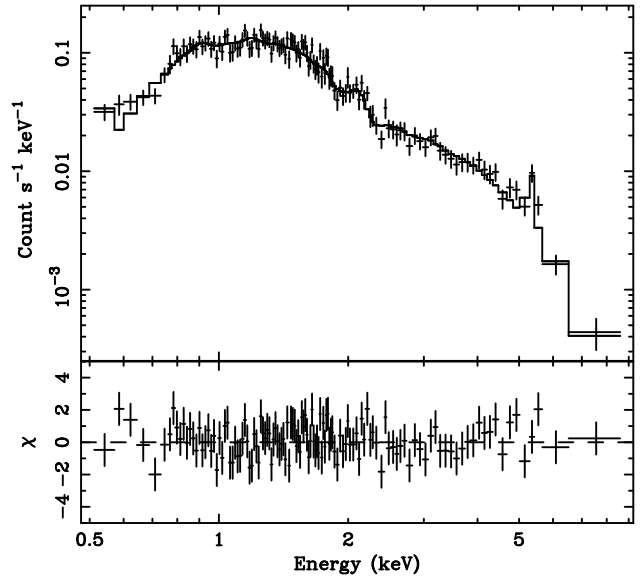

Figure 5. (Upper Panel) The S0 spectrum for Abell 1835 with the best-fit solution for Model B overlaid. (Lower Panel) Residuals to the fit. Details as in Fig. 4.

Table 11. Cluster mass distributions

	kT		σ		r_c
Zwicky 3146	$6.6^{+3.0}_{-0.7}$	$\left(^{+1.1}_{-0.7}\right)$	850^{+175}_{-50}	$\left(^{+60}_{-50}\right)$	45
Abell 1835	$9.5^{+4.9}_{-2.0}$	$\left(^{+1.3}_{-1.7}\right)$	1000^{+300}_{-100}	$\left(^{+150}_{-70}\right)$	50
E1455+223	$5.4^{+2.2}_{-1.1}$	$\left(^{+1.9}_{-0.7}\right)$	720^{+180}_{-70}	$\left(^{+150}_{-40}\right)$	45

Notes: A summary of the temperature constraints (in keV) and the velocity dispersions (in $\mathrm{km\,s^{-1}}$) and core radii (in kpc) of the isothermal mass distributions (Binney & Tremaine 1989) required to produce the flat temperature profiles shown in Figs. $7 - 9$(d). Errors on the temperatures give the the full range allowed by spectral models C and D. (The tighter constraints determined with model D alone are given in parentheses.) Errors on the velocity dispersions show the range of values required to match the temperature results.

Figure 6. (Upper Panel) The S0 spectrum for E1455+223 with the best-fit solution for Model B overlaid. (Lower Panel) Residuals to the fit. Details as in Fig. 4.
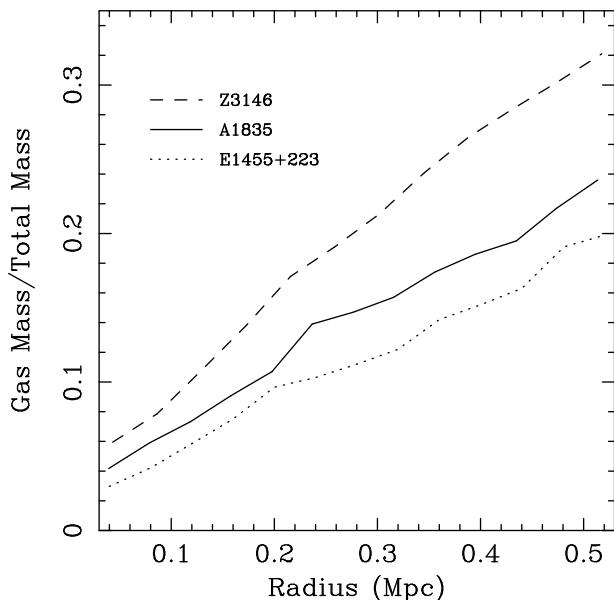
Figure 10. The ratio of the gas mass to the total mass as a function of radius.

absorption. This can have a significant effect on the mass deposition rates determined from the deprojection analyses.

To correct the deprojection results for intrinsic absorption, we adopt spectral model D as the most reasonable description for the clusters. The intrinsic column densities in Abell 1835 and E1455+223 ($N_{\rm H} = 3.8 \times 10^{21}$ atom cm^{-2}; Table 8) are assumed to be in uniform screens in front of the cooling flows. The effects of absorption on the observed HRI count rates from the cooling flows have been calculated from XSPEC simulations, using the ROSAT HRI response matrix issued by GSFC. For both Abell 1835 and E1455+223, the intrinsic absorption acts to reduce the count rates from the cooling flows by a factor of two (in detail, factors 2.07 and 2.04, respectively). The true mass deposition rates from the cooling flows can therefore be assumed to be a factor 2 larger than the values listed in Table 10. [For Zwicky 3146, the maximum allowed intrinsic column density of 10^{21} atom cm^{-2} implies a maximum correction factor to the mass deposition rate of 1.28.] The absorption-corrected mass deposition rates for the clusters are summarized in Table 12. The agreement between these values and the spectrally-determined mass deposition rates (Model D) is excellent.

6 OPTICAL PROPERTIES OF THE CLUSTERS

6.1 The galaxy populations

The galaxy populations in Abell 1835 and E1455+223 have been studied using the Palomar B and I images of the clusters. The SExtractor software of Bertin (1995) was used to identify galaxy candidates from their total (Kron) I magnitudes and $(B - I)$ colours (measured in 3.0 arcsec diameter apertures from seeing-matched images). For Abell

1835, 283 objects were selected with $15.0 < I < 21.0$ and $2.5 < (B - I) < 3.2$. The CCG (which is bluer than allowed by this range) was also included, making 284 galaxy identifications in total. For E1455+223, 188 objects with $15.0 < I < 21.0$ and $1.8 < (B - I) < 2.7$ were identified. Absolute V magnitudes were calculated from the observed I magnitude, and applying the appropriate K-corrections.

In Figs. 11 (a), (b) we plot the (projected) galaxy profiles and the ratio of the galaxy mass to the total mass for Abell 1835 and E1455+223. A value for $(M/L)_V$ of 10 has been assumed. Note the large central peaks in the ratio profiles [Fig. 12(b)] due to the luminous central galaxies, and the near-flatness of the ratios at large radii ($r \gtrsim 0.5$ Mpc) indicating that the galaxies follow an approximately isothermal distribution.

6.2 Spectra of the central cluster galaxies

Optical spectra for the CCGs of Zwicky 3146 and Abell 1835 are presented and discussed by Allen (1995). These CCGs are two of the most optically line-luminous central galaxies known, with luminosities in H$\alpha\lambda$6563 emission alone of $\sim 10^{43}$ erg s^{-1}. In Fig. 13 we present the spectrum of the CCG in E1455+223. The data were obtained with the Faint Object Spectrograph on the Isaac Newton Telescope (INT) in June 1991. A slit width of 1.5 arcsec was used, providing a resolution of ~ 16 Å in the first spectral order.

The CCG of E1455+223 exhibits strong, narrow emission lines (FWHM ~ 500 km s^{-1}) and an enhanced blue continuum with respect to a typical elliptical galaxy spectrum. Both features are characteristic properties of CCGs in large cooling flows (Johnstone, Fabian & Nulsen 1987; Heckman *et al.* 1992; McNamara & O'Connell 1989; Crawford & Fabian 1993; Allen 1995). The observed flux in H$\alpha\lambda$6563 of $1.9 \pm 0.1 \times 10^{-15}$ erg cm^{-2} s^{-1} implies a slit luminosity of $6.1 \pm 0.3 \times 10^{41}$ erg s^{-1}. However, the H$\beta\lambda$4861 emission line is only marginally detected and, after correcting for absorption by the underlying stellar continuum (a factor ~ 2 correction), we derive an H$\alpha\lambda$6563/H$\beta\lambda$4861 flux ratio of $\gtrsim 4.0$. This implies significant intrinsic reddening at the source $[E(B - V) \gtrsim 0.3]$ and an intrinsic H$\alpha\lambda$6563 (slit) luminosity of $\gtrsim 10^{42}$ erg s^{-1}. [The reddening laws of Seaton (1979) and Howarth (1983) have been used.] Donahue, Stocke and Gioia (1992) present results from a narrow-band Hα+[NII] imaging study of E1455+223. These authors show that the line emission from the CCG is highly extended and that the total line flux exceeds the slit flux reported here by a factor $\sim 7 - 8$. The Donahue *et al.* (1992) results, together with the spectral results reported here, thus imply an H$\alpha\lambda$6563 luminosity for the CCG of E1455+223 of $\gtrsim 7 \times 10^{42}$ erg s^{-1}, comparable to that of Zwicky 3146 and Abell 1835.

The CCGs of Zwicky 3146 and Abell 1835 also exhibit significant intrinsic reddening. In Table 12 we summarize the results on intrinsic X-ray absorption and optical reddening for the clusters. These results, together with the optical/X-ray/UV results discussed by Allen *et al.* (1995) for a larger sample of cooling flows at intermediate redshifts ($z \sim 0.15$), indicate an interesting tendency for clusters with large column densities of intrinsic X-ray absorbing material to exhibit significant intrinsic reddening. The similarity of the column densities inferred from the X-ray, optical and UV data, across a variety of aperture sizes, suggests a dust-to-
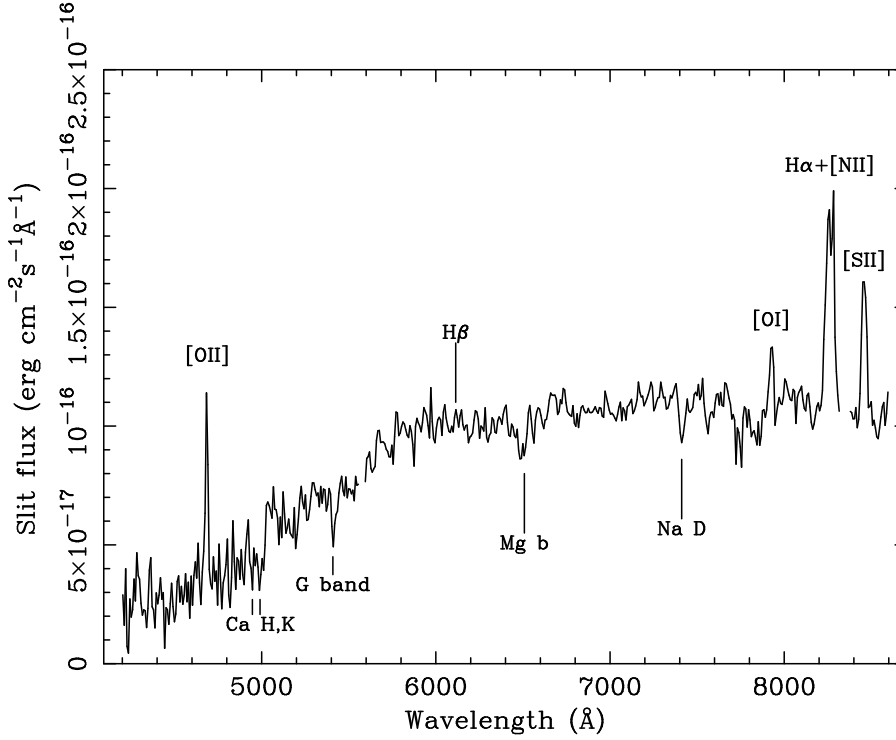
Figure 12. Optical spectrum of the CCG of E1455+223 obtained with the Faint Object Spectrograph on the INT in June 1991.

Table 12. Reddening and Excess absorption

	$N_{\mathrm{H,X-ray}}$	Spectral $\dot{M}$	Corrected deproj. $\dot{M}$	$E(B-V)$	$N_{\mathrm{H,OPT}}$
Zwicky 3146	< 1.0	1330^{+1220}_{-820}	1355^{+637}_{-161}	$0.22^{+0.15}_{-0.14}$	$1.3^{+0.9}_{-0.8}$
Abell 1835	$3.8^{+1.6}_{-0.4}$	2090^{+630}_{-700}	2291^{+943}_{-881}	$0.49^{+0.17}_{-0.15}$	$2.8^{+1.0}_{-0.9}$
E1455+223	$3.8^{+2.0}_{-0.8}$	2040^{+720}_{-880}	1491^{+330}_{-130}	$\gtrsim 0.3$	$\gtrsim 1.7$

Notes: Columns 2 and 3 list the intrinsic X-ray column densities (without account for systematic uncertainties in the SIS calibration; Section 4.3) and mass deposition rates determined from the spectral analysis of the combined instrument data sets (Table 8). Column 4 lists the mass deposition rates, determined by deprojection, corrected a posteriori for the effects of X-ray absorption (Section 5.3). For Zwicky 3146, zero intrinsic absorption has been assumed. Applying the maximum allowed correction factor for this cluster (1.28) gives a mass deposition rate of 1734^{+815}_{-206}. $E(B-V)$ estimates in column 5 are determined from the $H\alpha6563/H\beta4861$ line ratios in the CCGs. The data for Zwicky 3146 and Abell 1835 are from Allen (1995). $N_{\mathrm{H,OPT}}$ values are the column densities of X-ray absorbing material implied by the $E(B-V)$ estimates, following the relation of Bohlin, Savage & Drake (1978).

gas ratio in these galaxies similar to that in our own Galaxy. The results also suggest that much of the dust may be associated with, or entrained within, the X-ray absorbing gas.

7   DISCUSSION

We have discussed, in detail, the X-ray properties of Zwicky 3146, Abell 1835 and E1455+223. We have shown that all three of these clusters contain exceptionally large cooling flows. Zwicky 3146 and Abell 1835 are amongst the most X-ray luminous clusters known (Table 2). The cooling flows

in these systems account for $\sim 15 - 20$ per cent of the total intrinsic luminosity in the $2 - 10$ keV band, and as much as ~ 40 per cent in the $0.1 - 2.4$ keV ROSAT band. With E1455+223, which is a factor $2 - 3$ less luminous than the other clusters, the cooling flow accounts for ~ 35 per cent of the luminosity in 2-10 keV band and ~ 60 per cent of the emission between 0.1 and 2.4 keV.

Both Abell 1835 and E1455+223 exhibit significant intrinsic absorption in their ASCA spectra. The need for excess absorption is found in both the single-phase and multiphase (cooling flow) spectral analyses and cannot reasonably be attributed to uncertainties in the Galactic column den-
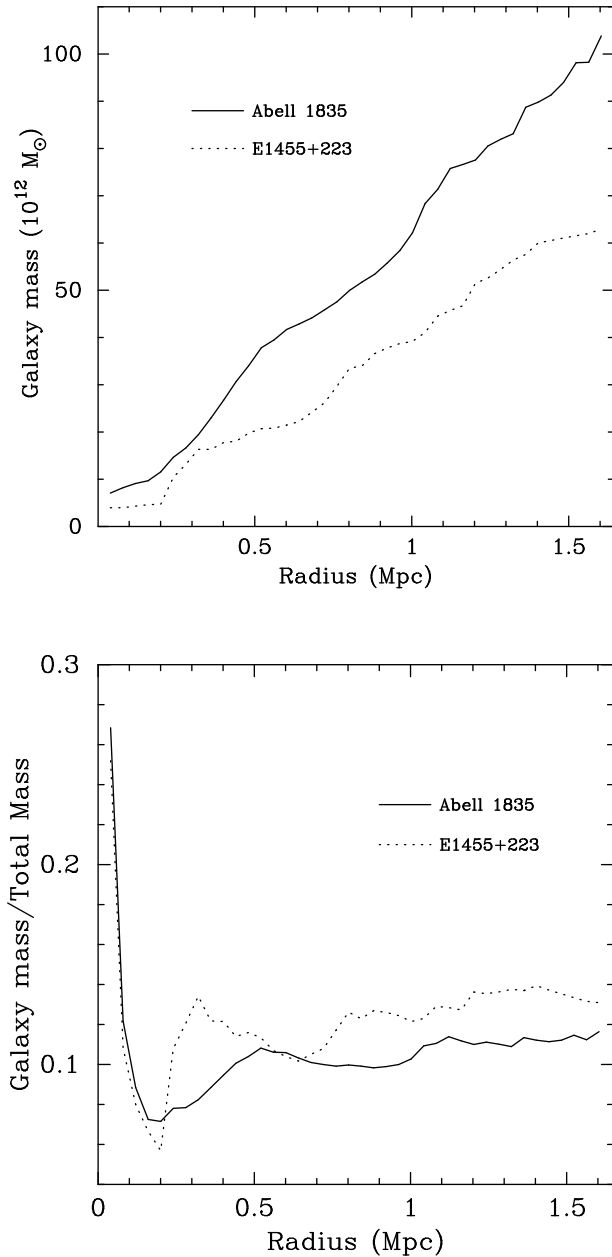
Figure 11. (a) The projected galaxy mass as a function of radius in Abell 1835 and E1455+223. (b) The ratio of the galaxy mass to the total mass (derived using the temperature constraints from spectral Model D).

sities (Stark *et al.* 1992). The most plausible interpretation of the excess absorption is that it is due to material associated with the cooling flows (spectral Model D). The mass of absorbing gas implied by an intrinsic column density of $\sim 3.8 \times 10^{21}$ atom cm^{-2}, distributed in a uniform (circular) screen across the central 220 kpc (radius $\sim r_{\rm cool}$) of the clusters, is $\sim 4.6 \times 10^{12}$ M$_\odot$. Such a mass could plausibly be accumulated by the cooling flows in Abell 1835 and E1455+223 in $\sim 2 - 3 \times 10^9$ yr. [See also White *et al.* (1991) and Allen *et al.* (1993).] Note also the excellent agreement in the mass deposition rates for the cooling flows determined with the spectral and deprojection methods (Section 5.3) under this assumption for the distribution of absorbing gas. With spectral models B and C, wherein the excess absorption is assumed to cover the whole cluster, the mass of absorbing gas is implausibly high. The intrinsic column densities inferred for Abell 1835 and E1455+223 are similar to those observed in nearby cooling flows (White *et al.* 1991; Allen *et al.* 1993; Fabian *et al.* 1994; Fabian *et al.* 1996). Note also that the metallicities of $Z \sim 0.25 - 0.30 Z_\odot$ measured for these clusters are similar to those observed in nearby systems, and imply that the the bulk of the enrichment of the ICM in these clusters occurred before redshifts of ~ 0.3.

7.1   Cooling flows and multiphase models

One of the most important results from this paper is the marked difference in the temperatures of the clusters determined from the single-phase and multiphase spectral models. These results are summarized in Table 13. The single-phase temperatures consistently (and significantly) underestimate the multiphase results. For Zwicky 3146 and Abell 1835, the ASCA single-phase results underestimate the multiphase temperatures by ~ 10 and 25 per cent, respectively. With the ROSAT data, the discrepancy in much more severe, with the PSPC values underestimating the ASCA multiphase results by ~ 3.4 keV (50 per cent) for Zwicky 3146, and ~ 6 keV (60 per cent) for Abell 1835. Note, however, that in all cases the reduced χ^2 values indicate statistically acceptable fits.

The multiphase kT results (Models C,D) should approximate the true mass-weighted temperatures in the clusters (Thomas *et al.* 1987; Waxman & Miralda-Escude 1995; Allen *et al.* 1996). The single-phase results, however, are simply emission/detector-weighted average values for the integrated cluster emission. Since the X-ray emissivity of cluster gas rises with increasing density (decreasing temperature), the presence of a large cooling flow naturally leads to a decrease in the emission-weighted temperature of a cluster. The effects on the emission-weighted kT are most dramatic in the $0.1 - 2.4$ keV band of the PSPC, where the emission from cooler gas phases dominates the detected flux. However, the (comparatively) poor spectral resolution and limited bandpass of the PSPC, mean that the single-phase models can still provide a statistically adequate description of the data. The PSPC data are unable to discern the need for multi-temperature components (although the imaging data clearly require them).

These results imply that caution should be applied in the interpretation of temperatures determined with simple, single-phase models and, in particular, those determined from ROSAT data. With ASCA data the single-phase re-

Table 13. Comparison of multiphase and single-phase results

Cluster	PSPC (SP)		ASCA (SP)		ASCA (MP)	
	kT	$\chi^2_\nu\ (\nu)$	kT	$\chi^2_\nu\ (\nu)$	kT	$\chi^2_\nu\ (\nu)$
Zwicky 3146	$3.2^{+1.4}_{-0.7}$	1.20 (22)	$6.1^{+0.3}_{-0.3}$	0.987 (870)	$6.6^{+1.1}_{-0.7}$	0.986 (866)
Abell 1835	$3.8^{+1.6}_{-0.9}$	0.85 (20)	$7.0^{+0.3}_{-0.3}$	0.950 (957)	$9.5^{+1.3}_{-1.7}$	0.936 (953)

Notes: A comparison of the temperature results obtained with the Single-phase (SP) and MultiPhase (MP) models. SP results from ASCA are for spectral Model B. MP results are for spectral Model D.

sults should be more reliable, although significant discrepancies can still arise (as in the case of Abell 1835).

The presence of a range of density and temperature phases is clearly established by the data for cooling flow clusters. However, it should not assumed that the absence of a cooling flow implies that a single-phase modelling of the ICM is appropriate. The existence of cooling flows with distributed mass deposition requires significant inhomogeneity (a density/temperature spread of $\sim$ a factor 2) in the ambient cluster gas before the cooling flow forms (Nulsen 1986; Thomas, Fabian & Nulsen 1987). The best data for clusters are consistent with such a range of inhomogeneity (Allen *et al.* 1992b). The absence of cooling flows in some nearby, luminous clusters such as the Coma cluster is usually attributed to merger events having disrupted the cluster cores and having re-heated and redistributed the cooling gas throughout the cluster. In such circumstances it seems unlikely that the merger will completely homogenize the gas and, therefore, that a single-phase model will provide an exact measure of the mass-weighted cluster temperature.

7.2   A comparison with lensing masses

In Fig. 13 we show the Palomar U band image of the central 2.5 arcmin^2 of Abell 1835. The CCG is the bright source in the centre of the field. The image shows a number of distorted features (arcs, arclets and image pairs) attributable to gravitational lensing by the cluster. In particular, we observe a bright, elongated arc ('A' in Fig. 13) at a radius of 30.3 arcsec from the centre of the CCG, along a PA of 133 degree. The arc has a length of $\sim$ 16 arcsec, is extended along a PA of 221 degree, and exhibits reflection symmetry about the point $14^{\rm h}01^{\rm m}03.7{\rm s}$, $02°52'21''$.

For a simple, circular mass distribution the projected mass within the tangential critical radius, $r_{\rm ct}$, is given by

$$M_{\rm proj}(r_{\rm ct}) = \frac{c^2}{4G} \left(\frac{D_{\rm arc}}{D_{\rm clus}D_{\rm arc-clus}} \right) r_{\rm ct}^2 \qquad (1)$$

where $r_{\rm ct}$ can be approximated by the arc radius ($r_{\rm arc} = 150$ kpc) and $D_{\rm clus}$, $D_{\rm arc}$ and $D_{\rm arc-clus}$ are respectively the angular diameter distances from the observer to the cluster, the observer to the lensed object, and the cluster to the lensed object. In Fig. 14 we show the mass within arc 'A' as a function of the redshift of the arc, calculated with the above formula. Also shown are the X-ray constraints on the projected mass within this radius [1.0×10^{14} M$_\odot$< $M_{\rm proj}$ < 2.1×10^{14} M$_\odot$ from the multiphase analysis using spectral

Model C, and 1.1×10^{14} M$_\odot$< $M_{\rm proj}$ < 1.6×10^{14} M$_\odot$ using spectral Model D]. Combining the X-ray and lensing mass results we are able constrain the redshift of arc 'A' to be > 0.7. It is also important to note that if the single-phase (Model B) X-ray temperature results for Abell 1835 were (wrongly) used in place of the multiphase values, no consistent solution for the X-ray and lensing masses would be possible.

The intrinsic ellipticity of the lensing potential may lead to a slight ($\lesssim$ 20 per cent) overestimate of the lensing mass determined with the circular mass model (Bartlemann 1995). However, the effects of ellipticity also lead to a slight overestimate of the X-ray mass within this aperture and, to first order, the conclusions on the redshift of the arc should not be dramatically affected. [The lensing properties of Abell 1835, and those of a larger sample of X-ray luminous clusters observed with the Palomar 5m telescope, are discussed further by Edge *et al.* (1996).]

Smail *et al.* (1995) report results from a study of (weakly) gravitationally distorted images in the field of E1455+223, from which they derive a projected mass within 450 kpc of the cluster centre of $\sim 3.6 \times 10^{14}$ M$_\odot$. This mass exceeds the X-ray determination of the projected mass within this radius, 1.6×10^{14} M$_\odot$ (for an isothermal mass distribution corresponding to a temperature of 5.4 keV), by a factor ~ 2. [Note that the determination of the X-ray mass assumes that the cluster remains isothermal and extends to 3Mpc. However, extrapolating the mass profile to 5 Mpc increases the projected mass within 450 kpc of the cluster centre by only ~ 2 per cent.] Using a potential consistent with the upper-limit to the X-ray temperature of 7.6 keV (*i.e.* $\sigma = 900$ km s^{-1}, $r_c = 40$ kpc) we still determine a projected mass within 450 kpc of only 2.5×10^{14} M$_\odot$.

The lensing result on the cluster mass for E1455+223 appears high. E1455+223 is a regular, relaxed cluster with a large cooling flow, and a $2 - 10$ keV X-ray luminosity of 1.3×10^{45} erg s^{-1}. The ASCA constraints on the X-ray temperature ($4.3 - 7.6$ keV) are consistent with results for other nearby, cooling-flow clusters of similar X-ray luminosity (*e.g.* Abell 1795; Edge *et al.* 1990, Fabian *et al.* 1996), which lends support to the X-ray mass determination. The velocity dispersion of $\sigma = 660 - 900$ km s^{-1} (Table 11) implied by the X-ray data is also in good agreement with optical observations ($\sigma \sim 700$ km s^{-1}; Mason *et al.* 1981, Smail *et al.* 1995).

A cluster of exceptional X-ray luminosity and temperature is required to provide a projected mass within

Figure 13. The Hale 5m U band image of Abell 1835. Arc 'A' is indicated to the South East of the CCG.

450 kpc consistent with the Smail *et al.* (1995) result for E1455+223. Abell 1835, discussed in this paper, provides a mass of $2.5 - 5.3 \times 10^{14}$ M$_\odot$. Similarly, the exceptionally X-ray luminous cooling-flow cluster PKS0745-191 ($L_X = 2.8 \times 10^{45}$ erg s^{-1}), for which Allen *et al.* (1996) present a self-consistent determination of the mass distribution from X-ray and gravitational lensing data, provides a projected mass within 450 kpc of only $\sim 3.7 \times 10^{14}$ M$_\odot$. Given the X-ray luminosity of E1455+223 (which is a factor 2-3 less than PKS0745-191 or Abell 1835), the X-ray mass measurement for the cluster seems reasonable and the lensing mass high. The result of Smail *et al.* (1995) may imply an unusual redshift distribution for the weakly distorted sources, or a projected mass distribution that deviates significantly from the simple isothermal mass model used (perhaps due to some line of sight mass enhancement from material external to the X-ray luminous part of the cluster).
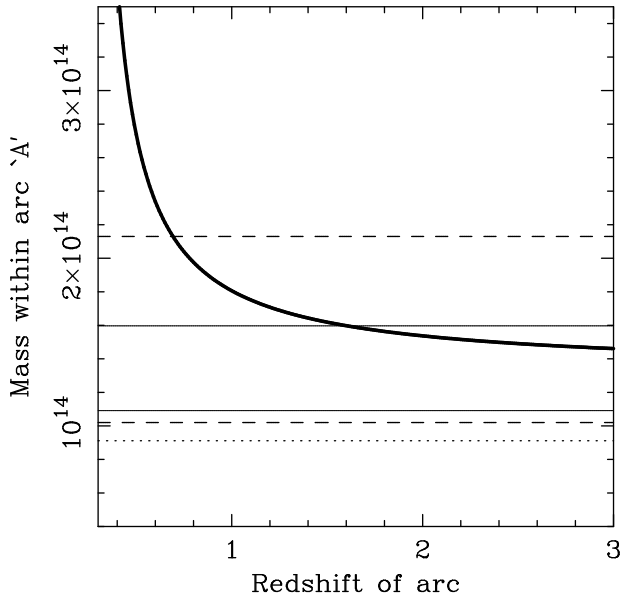
7.3 Optical and X-ray properties

CCGs in cooling flows frequently exhibit characteristic low-ionization, optical emission-line spectra (*e.g.* Johnstone, Fabian & Nulsen 1987; Heckman *et al.* 1989; Crawford & Fabian 1992; Allen *et al.* 1995). The optical (H$\alpha\lambda$6563) line luminosity correlates with the excess UV/blue continuum luminosity (the excess with respect to the UV/blue emission expected from a normal gE/cD galaxy; Johnstone, Fabian & Nulsen 1987; McNamara & O'Connell 1989; Allen *et al.* 1992a; Crawford *et al.* 1995; Allen 1995). Typically, both the emission lines and the excess UV/blue continua are extended across the central $10 - 20$ kpc of the clusters.

The clusters discussed in this paper contain three of the largest cooling flows known. They also host three of the most optically line-luminous (and UV/blue luminous) CCGs. Only the CCG of the massive cooling flow cluster PKS0745-191 exhibits a comparable optical line luminosity (Allen *et al.* 1996). Although no simple correlation between $\dot{M}$, t_{cool} and the optical line luminosity (and therefore UV/blue continuum luminosity) exists, the data presented here confirm a tendency for the most optically-line-luminous CCGs to be found in the largest cooling flows (*e.g.* Allen *et al.* 1995).

The UV/blue continua in Abell 1835 and Zwicky 3146 appear dominated by emission from hot, massive stars (Allen 1995). These young stellar populations may also provide the bulk of the ionizing continuum emission responsible for the observed optical emission lines. The exceptionally high mass deposition rates from the cooling flows in the clusters can naturally provide the large reservoirs of cooled material necessary to fuel the observed (very high) star formation rates (Allen 1995). The star formation may also account for some of the dust in the CCGs.

are used. We have discussed the relationship between intrinsic X-ray absorption and optical reddening in the clusters. These results suggest that the X-ray absorbing material frequently observed in the X-ray spectra of cooling flows is dusty.

REFERENCES

Allen S.W., 1995, MNRAS, 276, 947
Allen S.W., Fabian A.C., 1996, MNRAS, submitted
Allen S.W., Fabian A.C., Kneib J.P., 1996, MNRAS, 279, 615
Allen S.W. *et al.* 1992a, MNRAS, 259, 67
Allen S.W. Fabian A.C., Johnstone R.M., Nulsen P.E.J., Edge A.C., 1992b, MNRAS, 254, 51
Allen S.W., Fabian A.C., Edge A.C., Böhringer H., White D.A., 1995, MNRAS, 275, 741
Allen S.W., Fabian A.C., Johnstone R.M., White D.A., Daines S.J., Edge A.C., Stewart G.C., 1993. MNRAS, 262, 901
Anders E., Grevesse N., 1989, Geochemica et Cosmochimica Acta 53, 197
Bartelmann M., 1995, A&A, 299, 11
Bevington P.R., 1969, Data reduction and Error analysis for the Physical Sciences. McGraw-Hill, New York
Bertin E., 1995, SExtractor user's guide
Bohlin R.C., Savage B.D., Drake J.F., 1978, ApJ, 224, 132
Binney J., Tremaine S., 1987, Galactic Dynamics, Princeton Univ. Press, Princeton
Crawford C.S., Fabian, A.C. 1992, MNRAS, 259, 265
Crawford C.S., Fabian, A.C. 1993, MNRAS, 265, 431
Crawford C.S. *et al.* , 1995, MNRAS, 274, 75
Day C., Arnaud K., Ebisawa K., Gotthelf E., Ingham J., Mukai K., White N., 1995, the ABC Guide to ASCA Data Reduction, NASA GSFC
Donahue M., Stocke J.T., Gioia I.M., 1992, ApJ, 385, 49
Ebeling H., White D.A., Rangarajan F.V.N., 1996b, MNRAS, submitted
Ebeling *et al.* 1996a, MNRAS, submitted
Edge A.C., Stewart G.C., Fabian A.C., 1992, MNRAS, 258, 177
Edge A.C., Stewart G.C., Fabian A.C., Arnaud K.A., 1990, MNRAS, 245, 559
Edge A.C., Fabian A.C., Allen S.W., Crawford C.S., White D.A., Böhringer H., Voges W., 1994, MNRAS, 270, L1
Edge A.C., etal 1996, in preparation
Fabian A.C., Hu E.M., Cowie L.L., Grindlay J., 1981, ApJ, 248, 47
Fabian A.C., *et al.* 1996, in preparation
Fabian A.C., Arnaud K.A., Bautz M.W., Tawara Y., 1994, ApJ, 436, L63
Fabian A.C., 1994, A&AR, 32, 277
Heckman T.M., Baum S.A., Van Breugel W.J.M., McCarthy P., 1989, ApJ, 338, 48
Howarth I.D., 1983, MNRAS, 203, 301
Jedrzejewski R.I., 1987, MNRAS, 226, 747
Johnstone R.M., Fabian A.C., Edge A.C., Thomas P.A., 1992, MNRAS, 255, 431
Johnstone R.M., Fabian A.C., Nulsen P.E.J., 1987, MNRAS, 224, 75
Kaastra J.S., Mewe R., 1993, Legacy, 3, HEASARC, NASA

Figure 14. A comparison of the X-ray and lensing mass estimates for arc 'A'. The bold curve shows the mass within the arc determined from the standard lensing formula (for a spherical mass distribution) as a function of the redshift of the arc. The solid horizontal lines show the X-ray constraints on the mass within this radius determined with spectral Model D ($7.8 < kT < 10.8$ keV). The dashed lines show the constraints for spectral Model C ($7.5 < kT < 14.4$ keV). The lensing and multiphase X-ray results together imply $z_{\mathrm{arc}} > 1.6$ for Model D, and $z_{\mathrm{arc}} > 0.7$ for Model C. The lower dotted line shows the mass within arc 'A' implied by the single-phase spectral results ($M_{\mathrm{proj}} \sim 9.1 \times 10^{13}$ M$_\odot$ for $kT = 7.0$ keV). The single-phase X-ray results are inconsistent with the lensing data.

The excellent alignments between the (optical) CCG and (X-ray) cluster isophotes are consistent with the results for other massive cooling flows at intermediate ($z \sim 0.15$) redshifts (Allen *et al.* 1995). These results again reveal the unique and intimate link between CCGs and their host clusters.

8 CONCLUSIONS

We have presented detailed results on the X-ray properties of Zwicky 3146, Abell 1835 and E1455+223, three of the most distant, X-ray luminous clusters known. We have shown that these clusters contain the three largest cooling flows known, with mass deposition rates of $\sim 1400, 2300$ and 1500 M$_\odot$ yr^{-1}, respectively. We have presented mass models for the clusters and have highlighted the need for multiphase analyses to consistently explain the spectral and imaging X-ray data for these systems. The inappropriate use of single-phase models leads to significant underestimates of the cluster temperatures and masses. For Abell 1835 it was shown that a mass distribution that can consistently explain both the X-ray and gravitational lensing data for the cluster can only be formed when multiphase X-ray spectral models

Mason K.O., Spinrad H., Bowyer S., Reichert G., Stauffer J., 1981, AJ, 86, 803

McNamara B.R., O'Connell R.W., 1989, AJ, 98, 2018

Morrison R., McCammon D.M., 1983, ApJ, 270, 119

Nulsen P.E.J., 1986, MNRAS, 221, 377

Raymond J.C., Smith B.W., 1977, ApJS, 35, 419

Seaton M.J., 1979, MNRAS, 187, 75p

Shafer R.A., Haberl F., Arnaud K.A., Tennant A.F., 1991, XSPEC User's Guide,. ESA, Noordwijk

Smail I., Ellis R.S., Fitchett M.J., Edge A.C., 1995, 273, 277

Stark A.A., Gammie C.F., Wilson R.W., Bally J., Linke R.A., Heiles C. & Hurwitz M., 1992. ApJS, 79, 77

Thomas P.A., Fabian A.C., Nulsen P.E.J., 1987, MNRAS, 228, 973

Waxman E., Miralda-Escude J., 1995, ApJ, 451, 451

White D.A., Fabian A.C., Johnstone R.M., Mushotzky R.F., Arnaud K.A., 1991, MNRAS, 252, 72

White D.A., Fabian A.C., Allen S.W., Edge A.C., Crawford C.S., Johnstone R.M., Stewart G.C., Voges W., 1994, MNRAS, 269, 589